Redox Biology 87 (2025) 103869

Contents lists available at ScienceDirect

Redox Biology

journal homepage: www.elsevier.com/locate/redox

PARK7-driven IGF2BP3–K76 lactylation mediates ferroptosis and HAIC resistance in hepatocellular carcinoma

Zhiwen Zhu [a,1], Xinyu Xia [a,1], Yuanxiang Lu [c,1], Danfeng Li [a], Xincheng He [b], Baohua Zhang [b], Ge Xiong [b], Wanguang Zhang [a,*], Huifang Liang [a,**], Hong Zhu [b,***]

[a] Hepatic Surgery Center, Tongji Hospital, Tongji Medical College, Huazhong University of Science and Technology, Wuhan, 430030, China
[b] Department of Medical Oncology, The First Affiliated Hospital of Soochow University, Suzhou, 215006, China
[c] Department of Breast Surgery, Zhengzhou University People's Hospital, Henan Provincial People's Hospital, Zhengzhou, 450003, China

ARTICLE INFO

Keywords:
IGF2BP3
Lactylation
PARK7
Ferroptosis
Chemoresistance

ABSTRACT

Oxaliplatin/5-fluorouracil (OXA/5-FU)-based hepatic artery infusion chemotherapy (HAIC) represents a promising strategy against advanced hepatocellular carcinoma (HCC), yet acquired resistance frequently impedes its efficacy. Here, we identify lactylation of IGF2BP3 at lysine 76 (IGF2BP3–K76lac) as a key driver of HAIC resistance. IGF2BP3–K76lac overexpression enhances chemoresistance in vitro and in vivo. Mechanistically, lactylation at IGF2BP3 K76 strengthens its affinity for m6A-modified FSP1 mRNA, upregulating FSP1 and conferring ferroptosis resistance. Blocking of IGF2BP3–K76lac bolsters OXA/5-FU-induced ferroptosis, disrupts antioxidant defenses, and curbs tumor growth. Moreover, PARK7 functions as a lactyltransferase to facilitate IGF2BP3–K76lac via increasing the binding of lactate at IGF2BP3–K76 site. Finally, blocking antibody targeting IGF2BP3–K76lac was shown to work synergistically with OXA/5-FU to restore chemosensitivity. Taken together, our findings reveal a critical role for the PARK7–IGF2BP3–K76lac–FSP1 axis in HAIC resistance, highlighting IGF2BP3–K76lac as a potential therapeutic target in HCC.

1. Introduction

Hepatocellular carcinoma (HCC) is a leading cause of cancer-related mortality worldwide, primarily due to its advanced unresectable stage [1,2]. Current treatment options for advanced HCC include chemotherapy, targeted therapy, and immunotherapy, however, the efficacy remains limited [3–5]. Among these strategies, oxaliplatin/5-fluorouracil (OXA/5-FU)-based hepatic artery infusion chemotherapy (HAIC) has demonstrated potential in improving the objective response rate (ORR) and overall prognosis of HCC patients [6]. Nevertheless, drug resistance remains a major challenge, driven by mechanisms such as DNA damage repair, drug efflux, epigenetic modifications, and metabolic reprogramming [7,8]. Therefore, elucidating the mechanisms underlying resistance to OXA/5-FU-based HAIC is crucial for optimizing therapeutic outcomes.

Epigenetic regulation plays a critical role in controlling chemoresistance, especially the novel post-translational modifications (PTM) reported recently. Protein lactylation, a recently identified PTM mediated by metabolic processes, was first described in 2019 [9]. Traditionally, lactate was considered a metabolic byproduct with minimal biological significance. However, lactylation modifies histone lysine residues, thereby promoting transcriptional activation of specific genes involved in various pathological processes, including tumorigenesis, immunosuppression, and drug resistance [10–12]. N6-methyladenosine (m6A) is a predominant epigenetic modification that regulates mRNA stability and translation in eukaryotic cells [13]. Emerging evidence suggests that lactylation influences the function of m6A regulators, including writers, readers, and erasers, thereby affecting responses to

* Corresponding author. Hepatic Surgery Center, Tongji Hospital, Tongji Medical College, Huazhong University of Science and Technology, No. 1095 Jiefang Avenue, Wuhan, Hubei, 430030, China.
** Corresponding author. Hepatic Surgery Center, Tongji Hospital, Tongji Medical College, Huazhong University of Science and Technology, No. 1095 Jiefang Avenue, Wuhan, Hubei, 430030, China.
*** Corresponding author. Department of Medical Oncology, the First Affiliated Hospital of Soochow University, No. 899, Pinghai Road, Gusu District, Suzhou City, Jiangsu Province, 215006, China.
E-mail addresses: wgzhang@tjh.tjmu.edu.cn (W. Zhang), hfliang@tjh.tjmu.edu.cn (H. Liang), zhuhong_jasmine@suda.edu.cn (H. Zhu).
[1] These authors contributed equally: Zhiwen Zhu, Xinyu Xia, Yuanxiang Lu.

https://doi.org/10.1016/j.redox.2025.103869
Received 14 May 2025; Received in revised form 25 August 2025; Accepted 12 September 2025
Available online 26 September 2025

chemotherapy, targeted therapy, and immunotherapy [12,14,15]. The interaction between lactylation and m6A modification is increasingly recognized as a critical regulatory axis in cancer progression [11,16–18].

Ferroptosis, a form of iron-dependent programmed cell death, is distinct from apoptosis, necrosis, and autophagy. It is characterized by dysregulated iron homeostasis, impaired oxidative stress response, and excessive lipid peroxidation [19]. Ferroptosis has been identified as a promising mechanism to potentially overcome drug resistance in cancer therapy [20]. Furthermore, m6A reader insulin-like growth factor 2 mRNA-binding protein 3 (IGF2BP3) has been reported to be involved in the ferroptosis regulation and drug resistance [21,22]. We previously had confirmed that IGF2BP3 lactylation functions as a contributor in HCC lenvatinib resistance. Specifically, our previous work demonstrated that lactate accumulation in lenvatinib-resistant HCC cells contributes to IGF2BP3 K76 lactylation, which enhances PCK2 and NRF2 expression and promotes drug resistance [12]. However, the role of IGF2BP3 in HCC chemotherapy and immunotherapy, particularly in HAIC resistance, remains poorly understood. There is a need to investigate the intricate relationship between HAIC resistance, protein lactylation, m6A modification, and ferroptosis may provide new insights into the mechanisms of chemotherapy resistance and identify novel therapeutic targets.

In this study, we demonstrate that lactylation at lysine 76 of IGF2BP3 (IGF2BP3–K76lac) is upregulated in HAIC-resistant HCC and correlates with poor clinical prognosis. Integrative multiomic analysis highlighted a novel oncogenic epigenetic-modification axis PARK7–IGF2BP3–K76lac–FSP1 as a driver of ferroptosis resistance and chemoresistance. Functional validation in HCC cell lines and tumor-bearing mouse models confirms its role in tumor progression and chemoresistance. Moreover, a blocking antibody targeting IGF2BP3–K76lac, which exhibits therapeutic potential in both in vitro and in vivo models. Our findings highlight the PARK7–IGF2BP3–K76lac–FSP1 axis as a promising target for overcoming HAIC resistance in HCC.

2. Results

2.1. Elevated IGF2BP3–K76 lactylation is associated with chemoresistance in HCC

To evaluate whether IGF2BP3–K76lac mediates HAIC resistance in HCC, immunohistochemical analyses showed that IGF2BP3–K76lac levels were elevated in HCC patients resistant to OXA/5-FU-based HAIC. (Fig. 1A and B). Kaplan-Meier analysis indicated that patients with high IGF2BP3–K76lac levels had poor overall survival (Fig. 1C). Additionally, multivariate analysis showed that high IGF2BP3–K76lac expression was an independent risk factor for prognosis and HAIC resistance (Fig. 1D).

Next, following the IC50 heatmap that Hep3B and SNU-398 were selected as chemosensitive cell lines, and SNU-449 and SNU-423 were selected as chemoresistant cell lines to investigate the expression pattern of IGF2BP3–K76lac in HCC cells (Fig. 1E). Consistent with the heatmap analysis, the IC50 values of Hep3B and SNU-398 cells were significantly reduced after oxaliplatin or 5-fluorouracil treatment, while the IC50 values of SNU-449 and SNU-423 were higher (Fig. 1F). Furthermore, IGF2BP3–K76lac expression was analyzed in HCC cell lines, including Hep3B, C3A, SNU-398, SNU-423, SNU-378, SNU-449, Huh-7, and Huh-1. Notably, IGF2BP3–K76lac levels were significantly higher in chemoresistant cells than in chemosensitive cells (Fig. 1G). These findings suggest that IGF2BP3–K76lac may involved in resistance to OXA/5-FU-based chemotherapy.

2.2. IGF2BP3–K76 lactylation facilitates tumor growth via inducing chemoresistance

Next, we explored the functional role of IGF2BP3–K76lac in chemoresistance. We transfected Hep3B and SNU-398 cells with vector, $IGF2BP3^{WT}$ (wild-type of lactylation modification) overexpression plasmid, or $IGF2BP3^{K76R}$ (mutation at lysine 76 to arginine) plasmid. ShIGF2BP3 was transfected into SNU-449 and SNU-423 cells. Western blot analysis was used to detect the expression of IGF2BP3 (Fig. 2A and B). The IC50 values of these cells revealed a positive correlation between IGF2BP3–K76lac levels and chemoresistance. Overexpression of $IGF2BP3^{WT}$ increased the IC50 value of chemosensitive cells, while $IGF2BP3^{K76R}$ overexpression recovered the chemotherapy sensitivity (Fig. 2C). Conversely, IGF2BP3 knockdown reduced the IC50 values in chemoresistant cells following drug treatment (Fig. 2D). CCK-8 and colony formation assays showed that $IGF2BP3^{WT}$ overexpression promoted tumor growth and chemoresistance, while K76 mutation reversed chemoresistance, and IGF2BP3 knockdown inhibited HCC cell proliferation and chemoresistance (Fig. 2E–H). Additionally, the mutation of IGF2BP3–K76lac suppressed migration of HCC cells (Fig. S1A).

To assess whether IGF2BP3–K76lac mediated chemoresistance in vivo, we used a subcutaneous tumor model. $IGF2BP3^{WT}$ overexpression induced the chemoresistance, while $IGF2BP3^{K76R}$ overexpression eliminated the chemoresistance and reduced tumor volume and weight (Fig. 2I–K). These results suggest that IGF2BP3–K76lac promotes resistance to chemotherapy both in vitro and in vivo.

2.3. IGF2BP3–K76 lactylation desensitizes HCC cells to chemotherapy by inducing ferroptosis resistance

To uncover the molecular mechanism underlying IGF2BP3–K76lac-mediated chemoresistance, we performed transcriptomic RNA sequencing (RNA-seq) of Hep3B-$IGF2BP3^{WT}$ and Hep3B-$IGF2BP3^{K76R}$ cells. KEGG enrichment revealed significant enrichment of ferroptosis-related pathways (Fig. 3A). We hypothesize that IGF2BP3–K76lac may facilitates chemoresistance by promoting ferroptosis resistance.

To test this hypothesis we measured key ferroptosis indicators, including cell viability, lipid reactive oxygen species (lipid ROS), and mitochondrial morphology. Overexpression of $IGF2BP3^{WT}$ in Hep3B and SNU-398 cells conferred resistance to OXA-based chemotherapy. In contrast, $IGF2BP3^{K76R}$ overexpression significantly recovered OXA-induced growth inhibition and increased lipid ROS levels (Fig. 3B and C). Furthermore, RSL3, a classical inducer of ferroptosis [23], showed excellent antitumor effects when combined with oxaliplatin treatment (Fig. 3B and C). Conversely, the inhibitor of ferroptosis, liproxstatin-1, increased cell viability and decreased lipid ROS levels, suggesting that IGF2BP3–K76lac facilitates chemoresistance via inducing ferroptosis resistance (Fig. 3B and C). Electron microscopy revealed that $IGF2BP3^{WT}$ overexpression led to the reduction of oxaliplatin, RSL3 and combined therapy-induced rupture of the mitochondrial membrane and loss of mitochondrial cristae. Consistently, liproxstatin-1 impaired chemosensitivity induced by $IGF2BP3^{K76R}$ overexpression, presenting as the reduction of mitochondrial crest loss (Fig. 3D). To confirm these findings in vivo, immunohistochemistry showed that expression of 4-Hydroxynonenal (4-HNE) in the $IGF2BP3^{WT}$ group treated with oxaliplatin was significantly decreased (Fig. 3E). These results suggest that $IGF2BP3^{WT}$ enhances chemoresistance by inducing ferroptosis resistance in HCC cells.

2.4. IGF2BP3–K76 lactylation mediates FSP1 mRNA stability via m^6A modification

To investigate the mechanisms of IGF2BP3–K76lac in ferroptosis resistance, we integrated the RNA-seq results with the FerrDb database and RIP-Seq (Hep3B-$IGF2BP3^{WT}$ versus Hep3B-$IGF2BP3^{K76R}$) data. Focusing on the target gene ferroptosis suppressor protein 1 (FSP1/AIFM2), a known ferroptosis defender involved in chemoresistance (Fig. 4A). In addition, we identified highly enriched motifs within the m6A peak in Hep3B cells overexpressing $IGF2BP3^{WT}$ or $IGF2BP3^{K76R}$ plasmids using RIP-seq. (Fig. S2A). Western blot analysis showed that

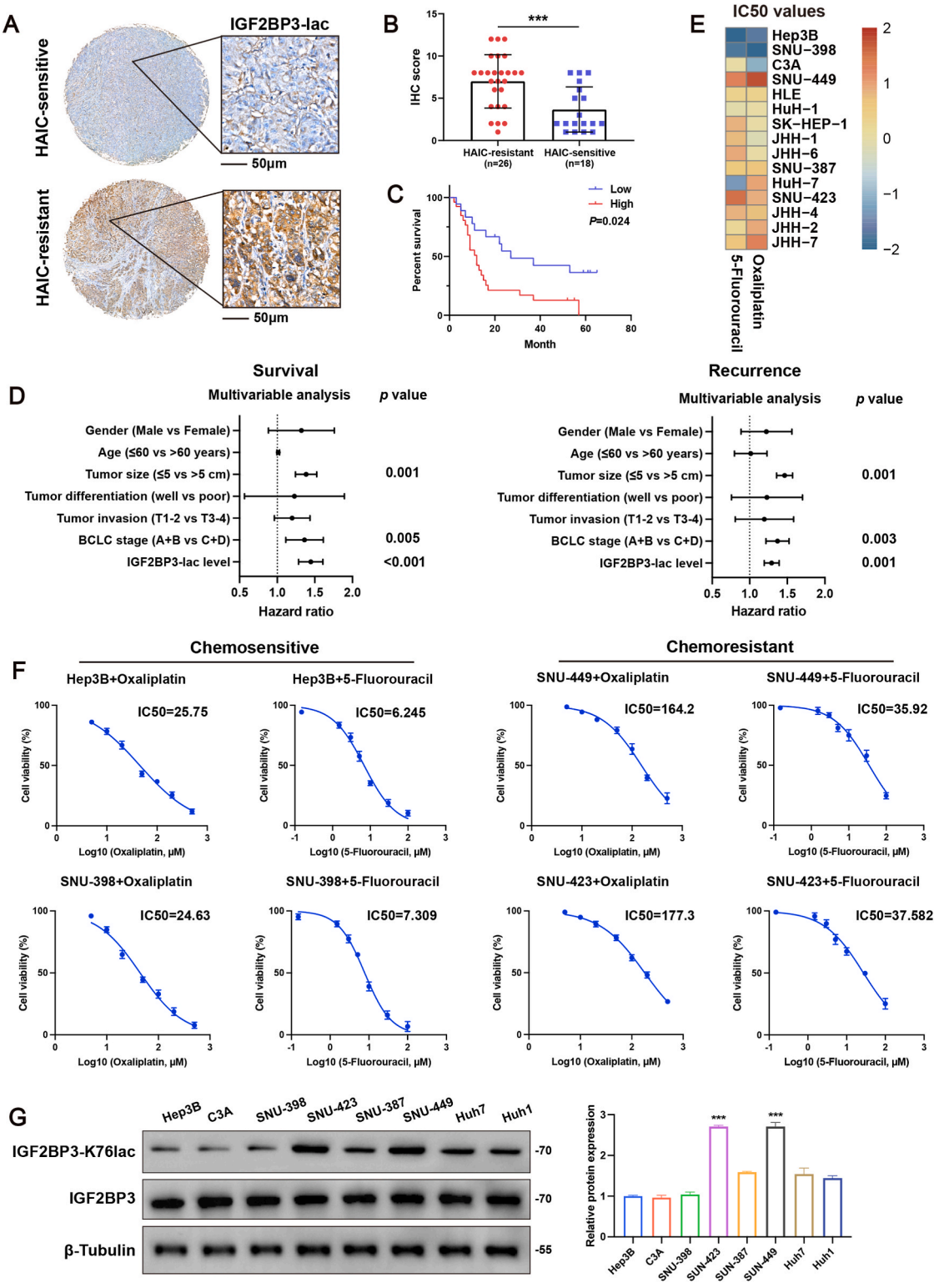

Fig. 1. IGF2BP3–K76 lactylation is upregulated in chemoresistant patients, and high IGF2BP3–K76lac correlates with poor prognosis. (A) Quantitative analysis of representative immunohistochemistry (IHC) images showing IGF2BP3–K76lac expression in HAIC-sensitive and HAIC-resistant tissues. (B) IHC scores reveal a strong correlation between IGF2BP3–K76lac levels and chemoresistance. (C) Kaplan-Meier analysis of overall survival in patients based on IGF2BP3–K76lac expression. (D) Multivariate analysis of survival and recurrence, highlighting IGF2BP3–K76lac as an independent risk factor for HCC. (E) Screening of chemosensitive and chemoresistant HCC cell lines using data from the Genomics of Drug Sensitivity in Cancer (GDSC) and the Cancer Therapeutics Response Portal (CTRP) databases. (F) IC50 values of chemosensitive and chemoresistant HCC cells treated with oxaliplatin or 5-fluorouracil for 24 h. (G) Western blot detection of IGF2BP3–K76lac expression in various HCC cell lines (n = 3). Statistical analysis was conducted using two-tailed unpaired Student's t-test or one-way analysis of variance (ANOVA) as appropriate. Error bars represent the mean ± SD (n = 3 independent experiments). *$p < 0.05$, **$p < 0.01$, ***$p < 0.001$.

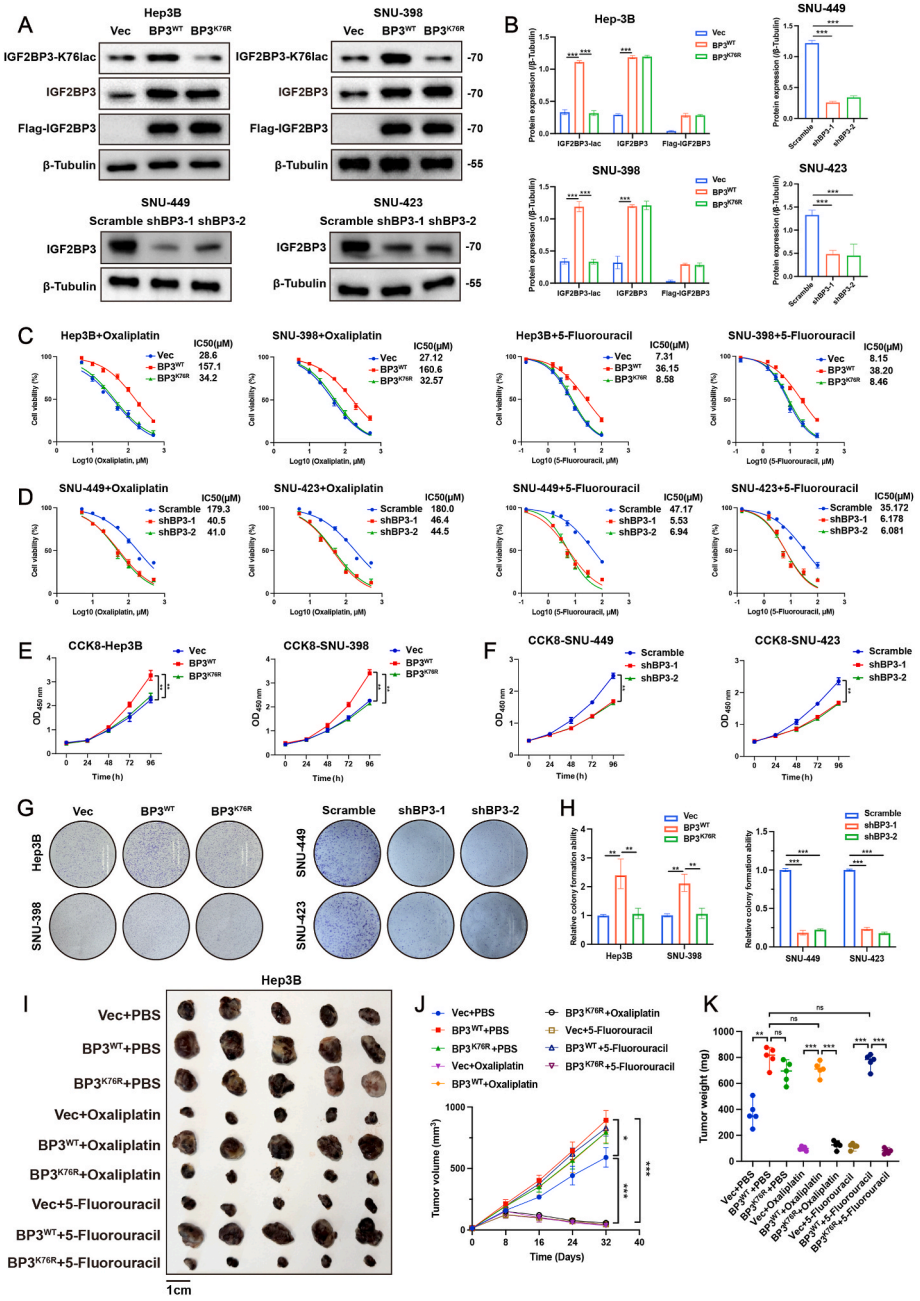

Fig. 2. IGF2BP3–K76 lactylation promotes chemoresistance. (A–B) Western blot analysis of protein expression in HCC cells transfected with IGF2BP3^{WT}, IGF2BP3^{K76R} plasmids, or infected with scramble and shBP3 lentiviruses (n = 3). (C–D) IC50 values of chemosensitive and chemoresistant HCC cells (n = 3). (E–F) Cell viability measured with the CCK-8 assay after treatment with oxaliplatin or 5-fluorouracil for 24 h (n = 3). (G–H) Colony formation assay measuring cell proliferation after oxaliplatin or 5-fluorouracil treatment for 24 h (n = 3). (I–K) Subcutaneous tumor growth in BALB/c nude mice (n = 5 per group) following treatment with vehicle (PBS), oxaliplatin (10 mg/kg), or 5-fluorouracil (10 mg/kg) daily. Tumor volumes and weights were monitored bi-daily. Statistical analysis was conducted using two-tailed unpaired Student's t-test or ANOVA as appropriate. Error bars represent the mean ± SD (n = 3 independent experiments). *$p < 0.05$, **$p < 0.01$, ***$p < 0.001$.

overexpression of IGF2BP3^{WT} increased FSP1 mRNA and protein levels in Hep3B and SNU-398 cells, while IGF2BP3^{K76R} overexpression reduced FSP1 expression in the same cells. IGF2BP3 knockdown reduced FSP1 expression in SNU-449 and SNU-324 cells (Fig. 4B; Fig. S2B).

We hypothesize that IGF2BP3 may modulate FSP1 through m6A modification. Through IHC staining we found that increased m6A levels in HAIC-resistant patients, underscoring the potential role of m6A in HAIC resistance (Fig. S2C). To assess the role of m6A modification in FSP1 mRNA, we used the SRAMP website to predict potential m6A modification sites, predicting a high-scoring sites (Fig. 4C). Integrative Genomics Viewer analysis revealed raised m6A peak enrichment in FSP1 mRNA in IGF2BP3^{WT} cells, suggesting that IGF2BP3–K76lac dynamically regulates FSP1 mRNA through m6A modification (Fig. 4D). Subsequently, in vitro RNA pull down assays revealed that m6A-modified FSP1 RNA probes bind to IGF2BP3 and that this interaction is disrupted by A-to-T point mutations at these m6A sites (Fig. S2D). RIP-qPCR analysis confirmed that FSP1 is a significant target of IGF2BP3–K76lac (Fig. 4E). The high activity of dual luciferase reporter was only observed in FSP1-WT group of IGF2BP3^{WT} overexpression, mutation of FSP1 did not affect the activity of dual luciferase reporter construct bearing IGF2BP3-CDS/UTR with K76 or KH3-4 mutations (Fig. 4F). IGF2BP3–K76lac levels increased upon IGF2BP3^{WT} overexpression,

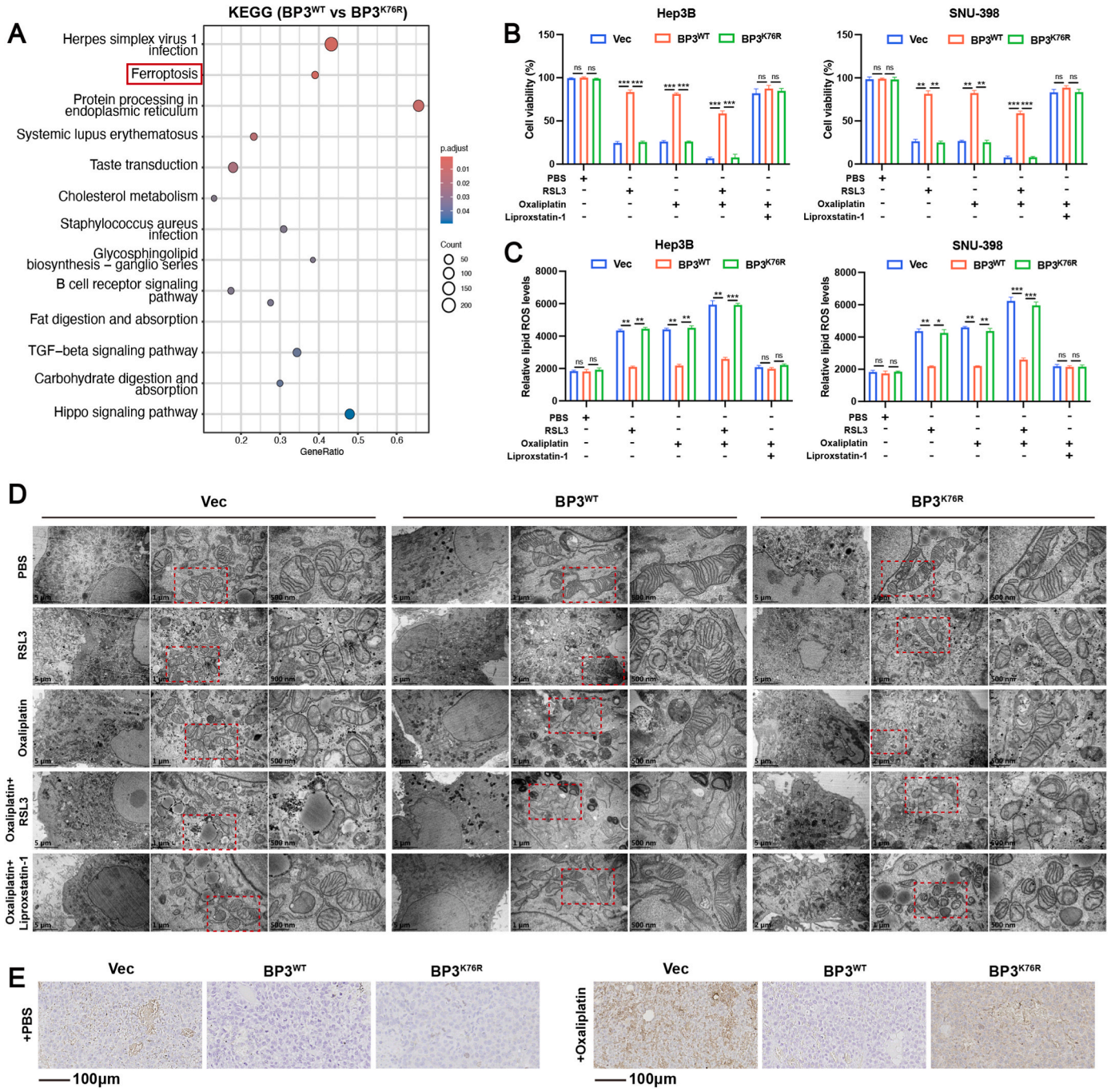

Fig. 3. IGF2BP3–K76 lactylation desensitizes HCC cells to chemotherapy by inducing ferroptosis resistance. (A) RNA-seq results showing enrichment of the ferroptosis pathway in KEGG analysis (Hep3B-IGF2BP3^{WT} and Hep3B-IGF2BP3^{K76R} treated with oxaliplatin for 24 h). (B) Cell viability measured with the CCK-8 assay after oxaliplatin, RSL3, oxaliplatin + RSL-3, oxaliplatin + liproxstatin-1 treatment for 24 h (n = 3). (C) Flow cytometry analysis of intracellular lipid ROS levels in HCC cells transfected with IGF2BP3^{WT} or IGF2BP3^{K76R} plasmids and treated with oxaliplatin, RSL3, oxaliplatin + RSL-3, oxaliplatin + liproxstatin-1 for 24 h (n = 3). (D) Representative electron microscopy images of mitochondrial morphology in Hep3B and SNU-398 cells treated with oxaliplatin, RSL3, oxaliplatin + RSL-3, oxaliplatin + liproxstatin-1 for 24 h. Red boxes indicate shrunken mitochondrial membranes and decreased or absent cristae. Scale bars: 5 μm, 2 μm, 1 μm, 500 nm. (E) Representative IHC images of 4-HNE in tumor tissues. Scale bar = 100 μm. Statistical analysis was conducted using two-tailed unpaired Student's t-test or ANOVA as appropriate. Error bars represent the mean ± SD (n = 3 independent experiments). *$p < 0.05$, **$p < 0.01$, ***$p < 0.001$.

while remained unchanged after FSP1 inhibition (Fig. 4G; Fig. S2E). Moreover, IGF2BP3^{WT} overexpression elevated the mRNA level of FSP1 expression, whereas K76 and KH3-4 mutations failed to raise the expression of FSP1 (Fig. 4H). Polysome fractionation analysis revealed a decrease in FSP1 mRNA in polysome fractions upon IGF2BP3 knockdown (Fig. 4I). Actinomycin D treatment showed that mRNA stability of FSP1 was enhanced in cells with IGF2BP3^{WT} overexpression (Fig. 4J).

To determine whether lactylation affects IGF2BP3 binding to m6A-modified mRNA, we transfected Flag-IGF2BP3^{WT}, Flag-IGF2BP3^{K76R}, or vector alone into IGF2BP3-knockdown cells supplemented with 25 mM Nala. Immunoprecipitation followed by Western blotting revealed that m6A-modified RNAs bound more abundantly to Flag-IGF2BP3^{WT} + Nala than to Flag-IGF2BP3^{WT} alone. Interestingly, IGF2BP3^{WT} overexpression with Nala, but not the lactylation-deficient IGF2BP3–K76 mutant, resulted in the highest lactylation levels and significantly more m6A-modified RNA binding (Fig. 4K). In summary, IGF2BP3 lactylation

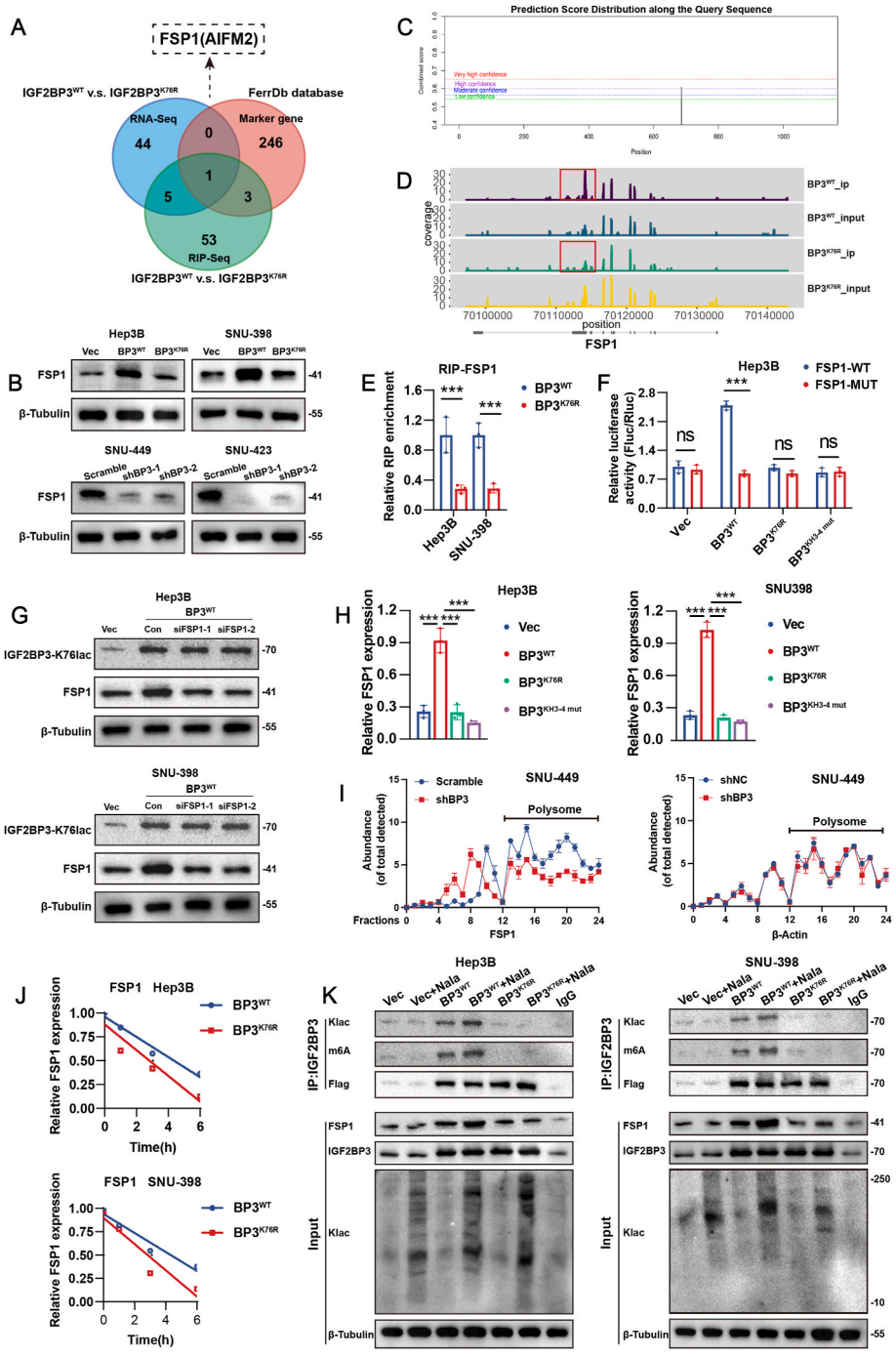

Fig. 4. IGF2BP3–K76 lactylation enhances FSP1 mRNA stability via m6A modification. (A) Venn diagram of RNA-seq, RIP-seq, and FerrDb database analysis showing differentially expressed genes from Hep3B cells overexpressing IGF2BP3^{WT} and IGF2BP3^{K76R}. (B) Western blot measurement of FSP1 protein expression in HCC cells (n = 3). (C) Prediction of m6A modification sites on FSP1 mRNA using SRAMP. (D) Gene plot representing FSP1 binding abundance in Hep3B cells overexpressing IGF2BP3^{WT} and IGF2BP3^{K76R}. (E) RIP-qPCR analysis of FSP1 mRNA levels in Hep3B and SNU-398 cells (n = 3). (F) Relative luciferase activity in control or FSP1 mutation cells transfected with pG-BP3^{WT}, pG-BP3^{K76R}, or pG-BP3^{KH3-4} (n = 3). (G) Western blot analysis of IGF2BP3–K76lac and FSP1 expression after FSP1 inhibition in Hep3B-IGF2BP3^{WT} cells (n = 3). (H) FSP1 mRNA levels measured by qRT-PCR (n = 3). (I) Polysome fractionation detected by qRT-PCR (n = 3). (J) FSP1 degradation rate following IGF2BP3^{K76R} overexpression in chemosensitive cells treated with actinomycin D. (K) Flag-IGF2BP3^{WT} and Flag-IGF2BP3^{K76R} transfected into Hep3B/SNU-398 cells, followed by Nala (25 mM) treatment for 24 h and immunoprecipitation with anti-Flag antibody. Western blot for protein identification. Statistical analysis was conducted using two-tailed unpaired Student's t-test or ANOVA as appropriate. Error bars represent the mean ± SD (n = 3 independent experiments). *$p < 0.05$, **$p < 0.01$, ***$p < 0.001$.

mediated FSP1 mRNA stability by binding to m6A-modified RNAs.

2.5. PARK7 is identified as a critical writer for IGF2BP3–K76 lactylated modification

Above-mentioned results demonstrated that the regulation of FSP1 expression depends on IGF2BP3–K76lac. We next sought to identify a

specific regulator of IGF2BP3–K76lac. Using LC-MS/MS, we identified binding proteins of IGF2BP3 in stable IGF2BP3^{WT} and IGF2BP3^{K76R} cells (Fig. 5A). Among the top 20 binding proteins, PARK7, SUMO4, FGB, SND1, and RBP4 were confirmed to be involved in protein regulation (Fig. 5B) [24–28]. Given that PARK7 is involved in lactate transport, we supposed that PARK7 may function as a lactyltransferase. We then investigated whether IGF2BP3 and PARK7 interact. Co-immunoprecipitation assays revealed an endogenous interaction between IGF2BP3 and PARK7 (Fig. 5C). Pull-down assays showed that GST-fused PARK7 pulled down IGF2BP3 (Fig. 5D). Furthermore, HA-PARK7 overexpression significantly increased IGF2BP3–K76lac (Fig. 5E). Supplementation with Nala also enhanced IGF2BP3–K76lac, while PARK7 expression remained unchanged. Meanwhile, interference of PARK7 failed to raise the level of IGF2BP3–K76lac (Fig. 5F).

Next, we measured FSP1 expression following PARK7 overexpression (PARK7-OE). FSP1 levels were elevated in PARK7-OE cells, and global lactylation levels were also increased (Fig. 5G). We further assessed the regulation of PARK7 to IGF2BP3–K76lac. PARK7-OE upregulated FSP1 m6A and mRNA levels in IGF2BP3^{WT} cells, but not in IGF2BP3^{K76R} cells, indicating that PARK7 promotes the ability of RNA binding of IGF2BP3 via IGF2BP3–K76lac (Fig. 5H and I). We also assessed the impact of inhibiting PARK7on IGF2BP3 activity, the result demonstrates that PARK7 inhibition led to a significant decrease in IGF2PB3 activity (Fig. S2F). Finally, immunofluorescence confirmed the co-expression of PARK7 and IGF2BP3 in HCC patients with chemoresistance, and PARK7 protein levels were positively correlated with IGF2BP3–K76lac levels (Fig. 5J). Overall, these results demonstrate that PARK7 positively regulates IGF2BP3 stability via lactylation at K76.

2.6. Inhibition of the PARK7/IGF2BP3/FSP1 axis reverses chemoresistance inducing by IGF2BP3–K76lac

Next, we explored whether PARK7 and IGF2BP3 influence chemotherapy sensitivity in HCC cells by regulating FSP1. Through immunohistochemistry analysis, we found that PARK7 and FSP1 were significantly overexpressed in HAIC-resistant tissues (Fig. 6A). Western blot results showed that IGF2BP3^{WT} overexpression upregulated both IGF2BP3–K76lac and FSP1 levels, while PARK7 expression remained unchanged (Fig. 6B; Fig. S3A). As expected, siRNA-mediated knockdown of PARK7 or FSP1 reversed the enhancing effects of IGF2BP3^{WT} overexpression (Fig. 6B). Inhibition of PARK7 or FSP1 also impaired the contribution of IGF2BP3^{WT} overexpression to cell proliferation and ferroptosis resistance (Fig. 6C and D). FSP1 functions as an oxidoreductase, reducing CoQ to CoQH2, thereby protecting cells from ferroptosis [19,29]. We next measured CoQH2/CoQ and NADPH/NADP^{+} ratios. Overexpression of IGF2BP3^{WT} increased both the CoQH2/CoQ and NADPH/NADP^{+} ratios, and inhibition of PARK7 or FSP1 restored the ratios (Fig. 6E and F). Electron microscopy showed more membrane ruptures and disappearance of mitochondrial cristae in the siRNA treatment group compared with the control group (Fig. 6G and H). In summary, interference with the PARK7–IGF2BP3–K76lac–FSP1 axis restored the antitumor effects of chemotherapeutic drugs.

Furthermore, we assessed whether inhibiting PARK7 in vivo could enhance chemotherapy sensitivity. We constructed Park7-Control (Park7-Con) and Park7-knockout (Park7-KO) Hepa1-6-OXAR (Oxaliplatin resistant) HCC cell (Fig. S3B). Subsequently, Park7-Con/KO Hepa1-6-OXAR cells were inoculated into mice livers, the results showed that Park7 knockout significantly increased oxaliplatin sensitivity (Fig. 6I–K). IHC staining indicated that Park7 inhibition reduced the expresison of IGF2BP3-lac (Fig. S3C). Moreover, we also constructed orthotopic nude mouse model inoculated with PARK7-Con and PARK-KO Huh7 cells, the results are consistent with the above conclusion (Fig. S3D–E). Overall, inhibition of the PARK7/IGF2BP3/FSP1 axis presents a potential and promising approach for HCC chemoresistance.

2.7. Blocking antibody of IGF2BP3–K76lac enhances chemosensitivity in HCC cells

Based on the preceding results, we hypothesized that targeting IGF2BP3–K76lac could be a promising therapeutic strategy. Given that current inhibitors lack tumor specificity and systemic toxicity risks, therefore, we developed a blocking antibody targeting IGF2BP3–K76lac to treat chemoresistant cells. The combination of 1D11 (blocking antibody targeting IGF2BP3–K76lac) and chemotherapy showed a better antitumor effect in the group (Fig. 7A). Meanwhile, immunofluorescence revealed that the expression of 1D11 was significantly higher in chemoresistant patients than in chemosensitive patients (Fig. 7B).

Next, we investigated whether 1D11 could reverse the chemoresistance of IGF2BP3^{WT} overexpressing cells. We found that 1D11 alone had a stronger antitumor effect than chemotherapy treatment alone. The combination of 1D11 and chemotherapy exhibited an even greater antitumor effect (Fig. 7C). Both 1D11 alone and in combination with chemotherapy induced higher levels of lipid ROS compared with chemotherapy alone (Fig. 7D). Consistently, the tumor volumes were significantly reduced in the single and combination groups (Fig. 7E). Pathological and biochemical analysis showed that blocking antibodies had tolerable-toxic effect on mice liver (Fig. S4A–B). Immunohistochemical staining indicated that 4-HNE positive cells were enriched in both single 1D11 treatment and combination treatment groups (Fig. 7F). Moreover, in orthotopic model we found that the tumor weights were significantly reduced in the combination groups (Fig. S4C–D). In conclusion, blocking K76 lactylation effectively reversed chemoresistance in HCC cells.

3. Discussion

OXA/5-FU-based HAIC is an important treatment method for advanced HCC, however, approximately 54 % of patients exhibit poor responses due to acquired resistance [30]. Emerging evidence suggests that post-translational modifications (PTMs) play a pivotal role in modulating therapeutic resistance [31]. In this study, we identified IGF2BP3–K76lac as a key regulator of chemoresistance, demonstrating that its modification promotes insensitivity to chemotherapy by inhibiting ferroptosis. Mechanistically, IGF2BP3–K76lac was critical for RNA binding and facilitated the upregulation of FSP1 mRNA. Furthermore, we identified PARK7 as a novel lactyltransferase that catalyzes IGF2BP3–K76lac. Inhibition of IGF2BP3–K76lac restored sensitivity to HAIC-based chemotherapy, suggesting that targeting IGF2BP3–K76lac represents a promising therapeutic strategy for overcoming HAIC resistance in HCC.

Chemotherapeutic drugs exerts its antitumor effects primarily through the formation of DNA crosslinks, which disrupt DNA integrity and function [32]. Excessive DNA damage can induce cell-cycle arrest, various forms of programmed cell death, and epigenetic modifications [7,33]. However, under conditions of therapeutic stress, tumor cells undergo metabolic reprogramming, epigenetic remodeling, and microenvironmental adaptations to counteract DNA damage and sustain survival [7,8,34]. Protein lactylation, a recently identified PTM, modifies lysine residues in histones through lactate accumulation during glycolysis [9]. Increasing evidence suggests that lactylation contributes to drug resistance, particularly in chemotherapy, targeted therapy, and immunotherapy [10–12]. We previously demonstrated that IGF2BP3 lactylation as a contributor in the HCC progression [12]. In this study, we further explored the role of IGF2BP3–K76lac in chemotherapy resistance and DNA repair in HCC. Notably, IGF2BP3–K76lac was significantly elevated in HAIC-resistant patients, and its inhibition restored chemosensitivity both in vitro and in vivo. Unlike kinase-driven phosphorylation or chromatin-focused acetylation, IGF2BP3 lactylation integrates metabolic reprogramming with m6A-mediated RNA stability, creating a unique epigenetic-metabolic feedback loop in drug resistance. Targeting this axis may overcome resistance in metabolically

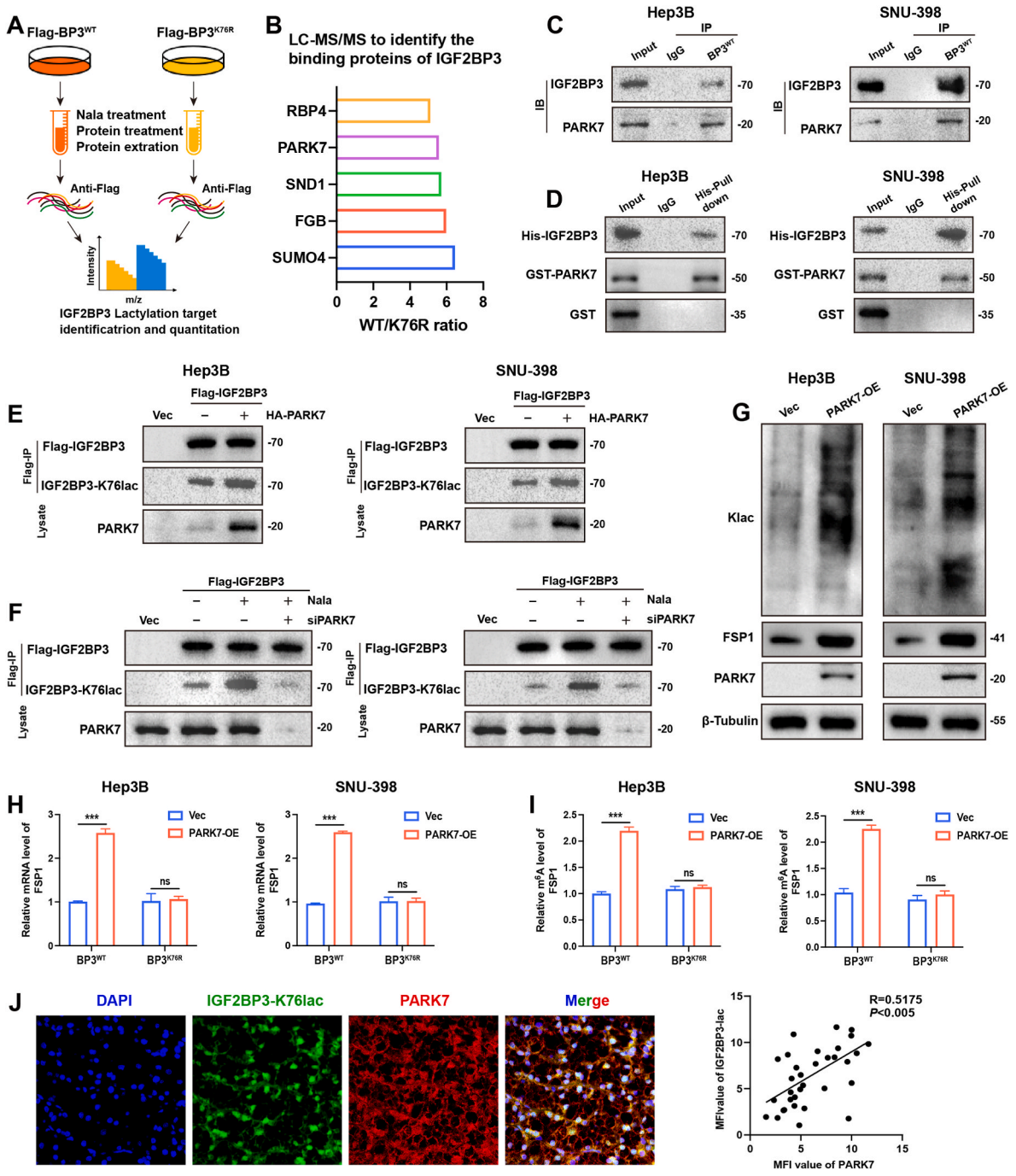

Fig. 5. Identification of PARK7 as a critical writer for IGF2BP3–K76 lactylation. (A) Workflow of the LC-MS/MS method used to identify IGF2BP3-interacting proteins. (B) The top binding proteins identified by LC-MS/MS assay. (C) Endogenous IGF2BP3 was immunoprecipitated using anti-IGF2BP3 antibody; IgG served as a negative control (mock IP). Co-precipitated PARK7 was detected by Co-IP. (D) Recombinant His-tagged IGF2BP3 was incubated with GST-PARK7 or GST proteins at 4 °C for 3 h, followed by His pull-down and Western blot. (E) Immunoprecipitation of cell lysates using Flag-IGF2BP3 beads, followed by Western blotting for total IGF2BP3 or lactylation using anti-Flag or IGF2BP3–K76lac antibodies. (F) Flag-IGF2BP3 plasmid was transfected into control or si-PARK7 cells with or without Nala treatment (25 mM, 24 h). (G) PARK7-OE plasmid was transfected into HCC cells, and protein levels were measured by Western blot. (H) PARK7-OE plasmid was transfected in IGF2BP3-WT/K76R overexpression cells, and FSP1 mRNA levels were measured by qRT-PCR (n = 3). (I) PARK7-OE plasmid was transfected in IGF2BP3-WT/K76R overexpression cells, and the relative m6A level of FSP1 was measured by MeRIP-qPCR (n = 3). (J) Immunofluorescent staining of HCC tissue containing HAIC-sensitive and HAIC-resistant tissues. Representative images showing the co-expression of IGF2BP3–K76lac and PARK7. Pearson correlation analysis of the mean fluorescence intensity (MFI) value between IGF2BP3–K76lac and PARK7 was measured by Image J ($R = 0.5715$ $p < 0.005$). Statistical analysis was conducted using two-tailed unpaired Student's t-test or ANOVA as appropriate. Error bars represent the means ± SD (n = 3 independent experiments). $^{*}p < 0.05$, $^{**}p < 0.01$, $^{***}p < 0.001$.

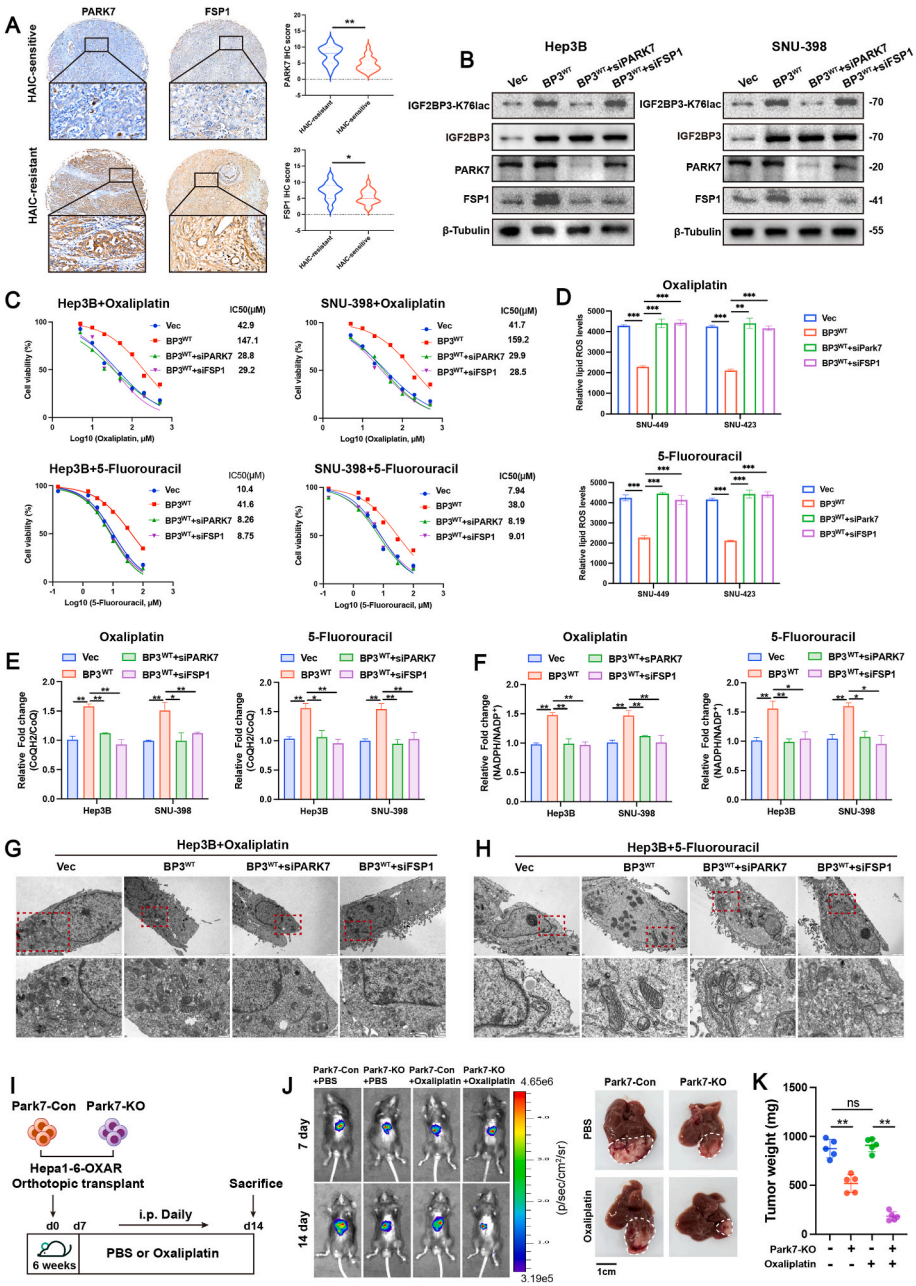

Fig. 6. Inhibition of the PARK7/IGF2BP3/FSP1 axis reverses chemoresistance inducing by IGF2BP3–K76lac. (A) Quantitative analysis of representative IHC images showing PARK7 and FSP1 expression in HAIC-sensitive and HAIC-resistant tissues. (B) Western blot analysis of IGF2BP3–K76lac, IGF2BP3, PARK7, and FSP1 expression following PARK7 or FSP1 inhibition in Hep3B/SNU398-IGF2BP3^{WT} cells. (C) Assessment of the impact of PARK7 or FSP1 inhibition on the IC50 values in Hep3B/SNU398-IGF2BP3^{WT} cells (n = 3). Treatment with oxaliplatin or 5-fluorouracil for 24 h. (D–F) Lipid ROS levels and the CoQH2/CoQ and NADPH/NADP^{+} ratios following PARK7 or FSP1 inhibition in Hep3B/SNU398 cells overexpressing IGF2BP3^{WT} (n = 3). (G–H) Representative electron microscopy images of mitochondrial ultrastructure. Red boxes indicate shrunken mitochondrial membranes, and decreased or absent mitochondrial cristae. Scale bars = 2 μm and 500 nm. (I) Timeline schematic of orthotopic mouse model. PBS/Oxaliplatin (10 mg/kg) treatment was initiated on day 7 after inoculation of tumor cells. (J–K) Representative IVIS luc fluorescence images of orthotopic mouse model inoculated with Control (Con) and Park7 knockout (KO) Hepa1-6-OXAR cells. (K) Statistical analysis of tumor weight (n = 5 per group). Statistical analysis was conducted using two-tailed unpaired Student's t-test or ANOVA as appropriate. Error bars represent the means ± SD (n = 3 independent experiments). *$p < 0.05$, **$p < 0.01$, ***$p < 0.001$.

dysregulated cancers. These findings align with recent studies indicating that lactylation of NBS1–K388 predicts poor prognosis in neoadjuvant chemotherapy, and its inhibition effectively reverses chemoresistance [35]. Collectively, these findings highlight lactylation as a crucial driver of drug resistance.

Cross-regulation among distinct PTMs is increasingly recognized as a key mechanism in cancer progression [36]. A recent study demonstrated that METTL16-K229 lactylation promotes cuproptosis in gastric cancer by enhancing m6A modification of FDX1 mRNA, while SIRT2 directly interacts with METTL16 to inhibit this process [16]. Furthermore, tumor-derived lactate facilitates METTL3 transcription via lactylation, contributing to an immunosuppressive tumor microenvironment through m6A-mediated regulation of JAK1 mRNA [11]. Ferroptosis, an iron-dependent form of regulated cell death, is characterized by extensive lipid peroxidation and oxidative stress [37]. A recent study has showen that lactate-driven upregulation of METTL3 enhances m6A

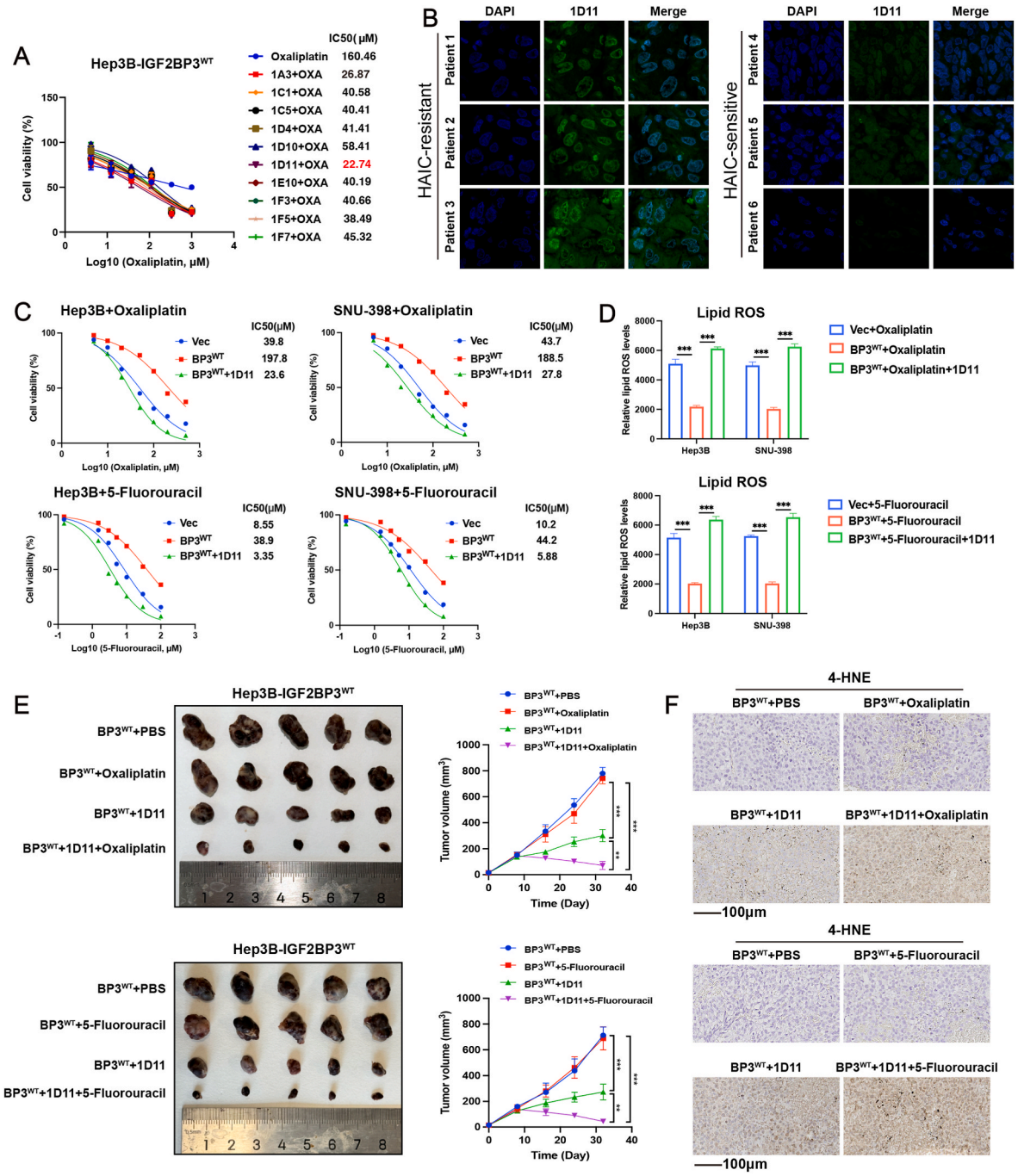

Fig. 7. Blocking antibody of IGF2BP3–K76 lactylation enhances chemosensitivity in HCC cells. (A) IC50 values of chemoresistant cells treated with IGF2BP3–K76lac blocking antibodies (n = 3). (B) Immunofluorescence detection the expression of IGF2BP3–K76lac antibody in HAIC-resistant and HAIC-sensitive HCC patients. (C) IC50 values of chemoresistant cells treated with IGF2BP3–K76lac blocking antibody or combined with chemotherapy (n = 3). (D) Flow cytometry analysis of intracellular lipid ROS levels (n = 3). (E) Representative tumor images post-therapy and quantification of tumor volume. Scale bar = 1 cm. IGF2BP3^{WT} overexpression cells were subcutaneously injected into the dorsal flanks of nude mice. Following tumor nodule formation, mice were administered PBS, Oxaliplatin (10 mg/kg), 5-fluorouracil (10 mg/kg), 1D11 (10 mg/kg) and combined treatments (10 mg/kg) once per 3 days via intraperitoneal injection (n = 5). (F) Representative IHC images of 4-HNE in tumor tissues. Scale bar = 100 μm. Statistical analysis was conducted using two-tailed unpaired Student's t-test or ANOVA as appropriate. Error bars represent the means ± SD (n = 3 independent experiments). *$p < 0.05$, **$p < 0.01$, ***$p < 0.001$.

modification of ACSL4 mRNA, thereby exacerbating ferroptosis-associated lung injury in sepsis [38]. Similarly, dexmedetomidine was shown to mitigate ferroptosis by reducing lactate production and downregulating MDH2 lactylation, thereby alleviating myocardial ischemia-reperfusion injury [39]. The cross-regulation among PTMs plays a pivotal role in regulating ferroptosis. Currently, we have deepened our analysis of lactate-driven metabolic rewiring in HCC. By integrating recent reports, we detail how glycolytic flux and lactate accumulation in HCC cells (e.g., via upregulated HK2 and c-MYC) not only promote immunosuppression but also modulate ferroptosis sensitivity by altering redox balance [40]. This includes links between ACLY inhibition and enhanced B cell-mediated antitumor immunity, providing a metabolic-immune perspective on ferroptosis regulation [41]. In the current study, we demonstrated that IGF2BP3 stabilizes

FSP1 mRNA via m6A modification, thereby protecting HCC cells from OXA/5-FU-induced ferroptosis. The FSP1/CoQ10 pathway serves as an endogenous antioxidant mechanism that neutralizes lipid peroxides, thereby inhibiting ferroptosis [29]. Our study further identified PARK7 as a lactyltransferase responsible for IGF2BP3–K76lac, which enhances m6A-mediated regulation of ferroptosis-related genes. These results highlight lactylation and m6A as interconnected epigenetic modifications that influence gene transcription and disease progression.

Another innovative work is that we developed a blocking antibody targeting IGF2BP3–K76lac. Currently, the development of pharmacological inhibitors targeting lactylation remains in its early stages, with a major challenge being the specificity of such inhibitors [42]. A deeper understanding of the molecular mechanisms governing lactylation in cancer is essential to advancing therapeutic interventions. Existing approaches to modulating lactylation primarily focus on inhibiting key enzymes and metabolic pathways [43,44]. Targeting lactylation-modulating enzymes, such as the SIRT family, or altering glycolytic flux has been proposed as a strategy to enhance the efficacy of existing therapies [45,46]. Preclinical studies have demonstrated the potential of these strategies in suppressing lactylation-driven tumorigenesis. However, the lack of tumor specificity and the risk of systemic toxicity pose significant obstacles to clinical translation [47]. In this study, we developed a blocking antibody targeting IGF2BP3–K76lac, which sensitized tumor cells to chemotherapy (Fig. 7). Notably, this antibody selectively targeted lactylated IGF2BP3 without affecting normal tissues, providing a promising avenue for therapeutic intervention.

Additionally, we observed that blocking PARK7 suppressed IGF2BP3–K76lac, thereby modulating ferroptosis-related pathways. PARK7, also known as Parkinson's disease protein 7 (DJ-1), is widely recognized for its role in oxidative stress response and mitochondrial homeostasis [48,49]. Recent studies have implicated PARK7 in cancer progression, particularly in regulating tumor metabolism and stress responses [50,51]. Although the functional significance of PARK7 lactylation remains unclear, ongoing research suggests that PTMs of PARK7 may influence its stability and activity [52]. Our findings indicate that PARK7-mediated lactylation of IGF2BP3 promotes ferroptosis resistance in HCC chemotherapy. However, we did not extensively investigate the downstream signaling pathways regulated by PARK7. Further studies are required to delineate the precise mechanisms underlying PARK7-dependent IGF2BP3 regulation.

In conclusion, this study verified that IGF2BP3–K76lac facilitate chemoresiatnce and ferroptosis resistance. Moreover, PARK7 was identified as a critical writer of IGF2BP3–K76lac, which in turn enhances FSP1 expression and promotes chemoresistance in HCC. Targeting IGF2BP3–K76lac presents a novel therapeutic strategy for overcoming HAIC resistance. Future research should explore the broader implications of lactylation in tumor progression, therapeutic resistance and ferroptosis regulation to refine targeted interventions for HCC.

4. Materials and methods

4.1. Tissue samples

Tumor paraffin sections were collected from patients who had undergone curative surgery for HCC at the Tongji Hospital. The specific procedures were performed according to a previous study [12]. All procedures were approved by the Ethics Committee of Tongji Hospital (TJ-IRB20230863) and were conducted in accordance with the Declaration of Helsinki and Istanbul. Informed consent was obtained from each patient. All animal studies were performed following a protocol approved by the Institutional Ethics Committee of Tongji Hospital.

4.2. Cell viability assay

Cells were seeded in 96-well plates (1×10^4 cells per well). Various concentrations of oxaliplatin or 5-fluorouracil were added for 24 h chemotherapy sensitivity was monitored at 450 nm by a microplate reader. The half-maximal inhibitory concentration (IC_{50}) was acquired by nonlinear regression in GraphPad Prism (version 8.0).

4.3. Cell culture and transfection

Human HCC cell lines Hep3B, SNU-398, SNU-449, and SNU-423 were purchased from Shanghai Institute of Cell Biology, Chinese Academy of Sciences. cells were cultured in MEM/DMEM supplemented with 10 % fetal bovine serum (Gibco, New York, USA). Cells were transiently transfected with siRNA and overexpression plasmids.

4.4. Quantitative real-time PCR (qRT–PCR)

Total RNA was isolated from tissues or cells utilizing the TRIzol reagent (Invitrogen, USA). Subsequently, complementary DNA (cDNA) was synthesized via a reverse transcriptase kit, following the protocol provided by the manufacturer. The reverse transcription of RNA into cDNA was carried out using a reverse transcriptase kit (Vazyme, Nanjing, China). Quantitative reverse transcription PCR (RT-qPCR) was conducted employing the FastStart Universal SYBR Green Master Mix (Vazyme) on a CFX Connect Real-Time System (BIO-RAD, California, USA), with β-Actin serving as the internal control. The relative mRNA expression levels were calculated using the $2-\Delta\Delta Ct$ method.

4.5. Western blot

Cells were collected and lysed in RIPA lysis buffer supplemented with a protease inhibitor cocktail (Sigma-Aldrich). Proteins (40 μg) were resolved on 10 % or 12 % SDS-PAGE gels and subsequently transferred onto PVDF membranes (Millipore, USA). Following blocking with 5 % nonfat milk, the membranes were incubated with primary antibodies. Protein detection was achieved using enhanced chemiluminescence reagents (Pierce, IL, USA). The specific antibodies utilized in this study are detailed in Table S5.

4.6. Colony formation assays

For the colony formation assays, 500 cells/well were seeded in a 6-well plate in triplicate. After 14 days of incubation, the plates were gently washed with PBS and stained with 0.1 % crystal violet.

4.7. Measurement of lipid reactive oxygen species (lipid ROS)

To evaluate lipid ROS production, cells were treated as specified, then stained with C11-BODIPY Lipid Peroxidation Sensor (Thermo Fisher; Cat #D3861) (Invitrogen) for 30 min at 37 °C in the dark. Excess C11-BODIPY was removed by washing the cells twice with PBS, and resuspended in PBS. The fluorescence intensity, indicative of lipid ROS levels was quantified by flow cytometry.

4.8. Dual luciferase assay

A dual luciferase reporter assay was conducted as previously outlined [12]. Luciferase activity was measured with the Dual-Luciferase R Reporter 1000 Assay System (Promega) with a GloMax 20/20 Luminometer (Promega) following the manufacturer's guidelines.

4.9. In vivo tumorigenesis

For Subcutaneous xenograft mouse model, four-week-old male BALB/c nude mice were obtained from the Gem Pharmatech Co. Ltd. (Jiangsu, China). Overexpression cells and control cells (5×10^6) were subcutaneously injected into the dorsal flanks of mice. Tumor volumes were measured every 4 days. The Ethics Committee of Tongji Hospital

approved these animal experiments. Animals were treated humanely following the guidelines specified in the "Guide for the Care and Use of Laboratory Animals". Mice were euthanized using CO_2 when their tumors and general health reached predetermined thresholds.

To establish an orthotopic xenograft mouse model, Park7-knockout HCC cells were generated by cloning single-guide RNAs (sgRNAs) (refer to Supplementary Table S1) into the lenti-CRISPR v2 vector. The plasmids (sgPark7-1/sgPark7-2, psPAX2, pMD2.G) were subsequently transfected into HEK293T cells. Viral supernatants were collected at 48 and 72 h post-transfection and concentrated using polyethylene glycol (PEG). These were then used to infect oxaliplatin (OXA)-resistant mouse HCC cells (Hepa1-6-OXAR) in the presence of polybrene. Following infection, puromycin selection was employed, and single-cell clones were expanded in 96-well plates. The knockout of Park7 was confirmed through sequencing of genomic DNA PCR products. Mice used in the study were between 6 and 8 weeks old. A total of 5×10^5 Park7 wild-type or knockout Hepa1-6-OXAR cells, suspended in 30 μL of PBS, were injected into the left hepatic lobe of six-week-old male mice. Oxaliplatin treatment commenced 7 days post-tumor cell inoculation. Intrahepatic tumor growth was assessed using bioluminescent imaging (IVIS Lumina II, Caliper, Princeton, NJ, USA).

4.10. Immunohistochemistry

Tissue sections were dewaxed in xylene and rehydrated with a series of descending graded alcohols. Rehydration was followed by a 15 min incubation in 3 % hydrogen peroxide to neutralize endogenous peroxidase activity. Antigen retrieval was performed using microwave heating for 15 min in a citric acid buffer. To prevent nonspecific binding, 10 % normal goat serum was applied. The sections were then incubated overnight at 4 °C with a primary antibody. Subsequently, a goat anti-rabbit secondary antibody was applied at room temperature for 30 min. Finally, the sections were treated with a diaminobenzidine working solution and counterstained with hematoxylin and covered with coverslips.

4.11. Immunofluorescence staining

Paraffin-embedded tissues containing HCC tissues and non-tumor tissues collected from the Tongji Hospital. The sections were dewaxed in xylene and rehydrated in descending graded alcohols. Triton X-100 (0.1 %) was used to increase antigen accessibility. Sections were blocked with 1 % bovine serum albumin for 1 h and incubated with primary antibodies overnight at 4 °C. Sections were washed with PBS and incubated with DyLight 594 or Alexfluor 488-labeled secondary antibody for 60 min at ambient temperature and stained with DAPI solution for 5 min. Immunofluorescence images were captured with a Zeiss confocal microscope.

4.12. Co-immunoprecipitation (Co-IP)

Cells were washed twice with phosphate buffered saline and lysed in radioimmunoprecipitation assay lysis buffer supplemented with protease inhibitor cocktail. The lysate was incubated with the indicated antibody for 3 h at 4 °C. Then A/G-plus agarose beads were added and the samples were rotated gently overnight at 4 °C. Finally, SDS-PAGE was performed to assess protein expression and association.

4.13. Glutathione S transferase (GST) pull-down

The cDNA encoding human PARK7 was cloned into the pET-42b vector. After transformation and amplification in E. coli BL21 (DE3) cells, GST-PARK7 fusion proteins were isolated using GST-affinity magnetic beads. For interaction assays, 5 μg of GST or GST-PARK7 was mixed with 5 μg of recombinant His-tagged IGF2BP3 protein (ABclonal Technology, China) in PBS and incubated at 4 °C for 4 h with continuous agitation. Protein complexes were immunoprecipitated using GST antibody-conjugated Protein A beads. Following three washes to remove unbound proteins, the captured complexes were resolved by SDS-PAGE and detected via Western blot.

4.14. Transmission electron microscope (TEM)

Cells were cultured in a 10-cm dish to 80–90 % confluency. The cell culture medium was discarded, and a pre-cooled electron microscopy fixative at 4 °C was immediately added to fix the cells for 1 h. Subsequently, the cells were gently scraped at a 45-degree angle using a cell scraper, ensuring not to scrape repeatedly. The collected cells were transferred to an appropriate centrifuge tube and centrifuged at 800–1000 rpm for 5 min. Most of the supernatant was discarded, and the cell pellet was resuspended and transferred to a 1.5 ml tube filled with electron microscopy fixative at 4 °C. Cells were fixed, embedded and sliced. Sections were double stained with uranyl acetate and lead citrate and visualized with a JEM-1400 electron microscope (JEOL, Japan).

4.15. RNA immunoprecipitation sequencing (RIP-seq) and RIP-qPCR assay

The process of RNA immunoprecipitation was done using the Magna RIP RNA-Binding Protein Immunoprecipitation Kit (Merck Millipore) along with an anti-IGF2BP3 antibody. Afterward, RNA was extracted and analyzed using quantitative PCR. Next-generation sequencing (NGS) involved preparing input and RIP samples, each with 150–200 ng of RNA. The NGS library was prepared using an Illumina Kit, and sequencing was carried out by SeqHealth Company, Wuhan, China.

4.16. Methylated RNA immunoprecipitation (MeRIP) qPCR assay

Methylation RNA immunoprecipitation (MeRIP) was conducted using the BersinBio MeRIP m6A kit (Guangzhou, China), following the manufacturer's instructions. First, RNA was extracted from HCC cells and fragmented using a lysis buffer at 94 °C for 5 min. Then the fragmented RNA was incubated overnight at 4 °C with magnetic beads precoated with anti-m^6A antibodies. After washing, the bead-antibody complex was mixed with DNA-free RNA. Finally, the RNA was eluted with the QI AGEN RNA extraction kit and analyzed by qPCR.

4.17. Polysome profiling

Polysome profiling was performed following the methodology described in a prior study. Hep3B and shIGF2BP3 cells were treated with 100 μg/mL cycloheximide (CHX) for 10 min at 37 °C. Subsequently, the cells underwent three washes with ice-cold CHX/PBS, followed by collection and lysis on ice for 10 min in a lysis buffer containing 20 mM Tris-HCl (pH 7.4), 10 mM MgCl2, 300 mM NaCl, 100 μg/mL CHX, 1 % Triton X-100, 1 mM DTT, 0.5 % sodium deoxycholate, 1 × RNase inhibitor, and 1 × EDTA-free protease inhibitor cocktail. The resulting lysate was centrifuged at 12,000×*g* for 10 min at 4 °C.

4.18. Transcriptomic RNA sequencing (RNA-seq)

RNA sequencing was performed by Vazyme Biotech Co. Ltd. (Nanjing, China). The specific procedures were according to a previous study [12].

4.19. LC-MS/MS analysis

Samples were analyzed on a Q Exactive HF-X mass spectrometer (Thermo Fisher, USA) coupled with an EASY-nLC 1200 system. Peptides were dissolved in 0.1 % formic acid (solvent A), loaded onto a trap column (100 μm × 2 cm, 3 μm/120 Å), and separated on a silica microcolumn (150 μm × 12 cm, 1.9 μm/120 Å) using a 75-min gradient

of 5–35 % solvent B (0.1 % formic acid in acetonitrile) at 600 nL/min. Full MS scans (300–1400 *m/z*, R = 120,000) with AGC 3e6 were followed by up to 20 dd-MS/MS scans (HCD, 27 % NCE, AGC 5e4, isolation window 1.6 *m/z*). Detection utilized an Orbitrap (R = 7500). Data were acquired via Xcalibur.

4.20. CoQH2/CoQ and NADPH/$NADP^+$ ratio quantification

According to the manufacturer's protocol, intracellular ubiquinone (CoQ) levels and the CoQH2/CoQ ratio were measured with the CoQ and $CoQH_2$ Assay Kit (SAINT-BIO, China). The absorbance of CoQ and $CoQH_2$ was measured at 620 nm using a microplate reader. The intracellular NADPH/$NADP^+$ ratio was quantified using the NADPH and $NADP^+$ Assay Kit (Beyotime, China) following the manufacturer's guidelines. The absorbance of $NADP^+$ and NADPH was measured at 450 nm using a microplate reader.

4.21. Scratch wound-healing assay

Transfected cells were cultured in 6-well plates until at least 90 % confluence. Cells were wounded with a 200 μL pipette tip and washed 3 times with PBS to remove detached cells. Images were captured at 0 h and 48 h and analyzed by Image J software.

4.22. RNA stability assay

HCC cell lines Hep3B/SNU-398 WT or K76R were seeded in 6-well plates. The cells were treated with actinomycin D (5 μg/mL, MCE) for 0, 3, 6, 9, and 12 h to inhibit transcription. At these time intervals, RNA was extracted and quantified using qPCR. The half-life of mRNA was calculated by linear regression based on RNA decay rates.

4.23. The development of blocking antibody targeting IGF2BP3–K76 lactylation

The development of blocking polyclonal antibody was commissioned to ABclonal Biotechnology Co., Ltd. (Wuhan, China). Briefly, the peptide C-EHSVPK (lac) RQRIR is dissolved in PBS buffer solution; Sulfur conjugated to KLH, immunized 3 rabbits, and then transferred for immunization. The antiserum was purified by antigen affinity using modified peptides and control peptides to obtain concentrated antibodies. The development of blocking monoclonal antibody was commissioned to Hangzhou HuaAn Biotechnology Co., Ltd. (Hangzhou, China). Briefly, the selected clones will be constructed into plasmids, transfected into HEK293 for antibody expression production, and purified using Protein A.

4.24. Statistics

The data are presented as means ± standard deviations. Statistical analysis to evaluate differences was conducted using Student's t-test. The relationship between IGF2BP3–K76lac and clinicopathological parameters was examined via the chi-square test. Statistical graphs were generated using GraphPad 8.0 software (GraphPad Software Inc., USA). $P < 0.05$ was considered statistically significance.

CRediT authorship contribution statement

Zhiwen Zhu: Writing – review & editing, Writing – original draft, Validation, Software, Investigation. **Xinyu Xia:** Writing – review & editing, Validation, Software, Investigation. **Yuanxiang Lu:** Writing – review & editing, Supervision, Methodology, Conceptualization. **Danfeng Li:** Writing – review & editing, Software. **Xincheng He:** Supervision, Software. **Baohua Zhang:** Writing – review & editing, Software. **Ge Xiong:** Supervision, Software. **Wanguang Zhang:** Writing – review & editing, Supervision, Resources, Investigation, Conceptualization. **Huifang Liang:** Writing – review & editing, Supervision, Conceptualization. **Hong Zhu:** Writing – review & editing, Supervision, Resources, Funding acquisition, Conceptualization.

Ethics approval and consent o participate

All procedures were approved by the Ethics Committee of Tongji Hospital and were conducted in accordance with the Declaration of Helsinki and Istanbul. Informed consent was obtained from each patient. All animal studies were performed following a protocol approved by the Institutional Ethics Committee of Tongji Hospital.

Financial Support

This work was supported in part by the National Natural Science Foundation of China (No. 82171834, No. 82573671, No. 82503881), the China Postdoctoral Science Foundation under Grant (2025M772151), Key Research and Development Program of Social Development of Jiangsu Province (No. BE2022725), the Suzhou Science and Technology Development Plan Project (No. SKY2023049) and Jiangsu Province Seventh 333 High Level (Second Level) Talents Project.

Declaration of competing interest

The authors declare the following financial interests/personal relationships which may be considered as potential competing interestsHong Zhu reports financial support was provided by National Natural Science Foundation of China. Reports a relationship with that includes:. Has patent pending to. If there are other authors, they declare that they have no known competing financial interests or personal relationships that could have appeared to influence the work reported in this paper.

Acknowledgements

We thank the patients and investigators who participated in the publicly available datasets for providing the data. We thank the Vazyme Biotech Co. Ltd., for their support with high-throughput technologies. This work was supported in part by the National Natural Science Foundation of China (No. 82171834, No. 82573671, No. 82503881), the China Postdoctoral Science Foundation under Grant (2025M772151), Key Research and Development Program of Social Development of Jiangsu Province (No. BE2022725), the Suzhou Science and Technology Development Plan Project (No. SKY2023049) and Jiangsu Province Seventh 333 High Level (Second Level) Talents Project.

Appendix A. Supplementary data

Supplementary data to this article can be found online at https://doi.org/10.1016/j.redox.2025.103869.

Data availability

Data from the Genomics of Drug Sensitibity in Cancer, (GDSC) (https://www.cancerrxgene.org) and the Cancer Therapeutics Response Portal, (CTRP) (https://portals.broadinstitute.org/ctrp) were downloaded.

References

[1] A. Vogel, T. Meyer, G. Sapisochin, R. Salem, A. Saborowski, Hepatocellular carcinoma, Lancet 400 (10360) (2022) 1345–1362.
[2] J.M. Llovet, R. Montal, D. Sia, R.S. Finn, Molecular therapies and precision medicine for hepatocellular carcinoma, Nat. Rev. Clin. Oncol. 15 (10) (2018) 599–616.
[3] J.M. Llovet, A. Villanueva, A. Lachenmayer, R.S. Finn, Advances in targeted therapies for hepatocellular carcinoma in the genomic era, Nat. Rev. Clin. Oncol. 12 (7) (2015) 408–424.

[4] J.M. Llovet, F. Castet, M. Heikenwalder, M.K. Maini, V. Mazzaferro, D.J. Pinato, et al., Immunotherapies for hepatocellular carcinoma, Nat. Rev. Clin. Oncol. 19 (3) (2022) 151–172.
[5] T.F. Greten, A. Villanueva, F. Korangy, B. Ruf, M. Yarchoan, L. Ma, et al., Biomarkers for immunotherapy of hepatocellular carcinoma, Nat. Rev. Clin. Oncol. 20 (11) (2023) 780–798.
[6] H. Iwamoto, S. Shimose, T. Shirono, T. Niizeki, T. Kawaguchi, Hepatic arterial infusion chemotherapy for advanced hepatocellular carcinoma in the era of chemo-diversity, Clin. Mol. Hepatol. 29 (3) (2023) 593–604.
[7] D. Jurkovicova, C.M. Neophytou, A. Gašparović, A.C. Gonçalves, DNA damage response in cancer therapy and resistance: challenges and opportunities, Int. J. Mol. Sci. 23 (23) (2022).
[8] Q. Wang, J. Liu, Z. Chen, J. Zheng, Y. Wang, J. Dong, Targeting metabolic reprogramming in hepatocellular carcinoma to overcome therapeutic resistance: a comprehensive review, Biomed. Pharmacother. 170 (2024) 116021.
[9] D. Zhang, Z. Tang, H. Huang, G. Zhou, C. Cui, Y. Weng, et al., Metabolic regulation of gene expression by histone lactylation, Nature 574 (7779) (2019) 575–580.
[10] J. Qu, P. Li, Z. Sun, Histone lactylation regulates cancer progression by reshaping the tumor microenvironment, Front. Immunol. 14 (2023) 1284344.
[11] J. Xiong, J. He, J. Zhu, J. Pan, W. Liao, H. Ye, et al., Lactylation-driven METTL3-mediated RNA m(6)A modification promotes immunosuppression of tumor-infiltrating myeloid cells, Mol Cell 82 (9) (2022) 1660–1677.e1610.
[12] Y. Lu, J. Zhu, Y. Zhang, W. Li, Y. Xiong, Y. Fan, et al., Lactylation-driven IGF2BP3-Mediated serine metabolism reprogramming and RNA m6A-Modification promotes lenvatinib resistance in HCC, Adv. Sci. (Weinh.) 11 (46) (2024) e2401399.
[13] K. Boulias, E.L. Greer, Biological roles of adenine methylation in RNA, Nat. Rev. Genet. 24 (3) (2023) 143–160.
[14] Y. Sun, W. Shen, S. Hu, Q. Lyu, Q. Wang, T. Wei, et al., METTL3 promotes chemoresistance in small cell lung cancer by inducing mitophagy, J. Exp. Clin. Cancer Res. 42 (1) (2023) 65.
[15] Y. Pan, H. Chen, X. Zhang, W. Liu, Y. Ding, D. Huang, et al., METTL3 drives NAFLD-Related hepatocellular carcinoma and is a therapeutic target for boosting immunotherapy, Cell Rep. Med. 4 (8) (2023) 101144.
[16] L. Sun, Y. Zhang, B. Yang, S. Sun, P. Zhang, Z. Luo, et al., Lactylation of METTL16 promotes cuproptosis via m(6)A-modification on FDX1 mRNA in gastric cancer, Nat. Commun. 14 (1) (2023) 6523.
[17] Y. Zhou, J. Yan, H. Huang, L. Liu, L. Ren, J. Hu, et al., The m(6)A reader IGF2BP2 regulates glycolytic metabolism and mediates histone lactylation to enhance hepatic stellate cell activation and liver fibrosis, Cell Death Dis. 15 (3) (2024) 189.
[18] W. Du, S. Tan, Y. Peng, S. Lin, Y. Wu, K. Ding, et al., Histone lactylation-driven YTHDC1 promotes hepatocellular carcinoma progression via lipid metabolism remodeling, Cancer Lett. (2024) 217426.
[19] S.J. Dixon, K.M. Lemberg, M.R. Lamprecht, R. Skouta, E.M. Zaitsev, C.E. Gleason, et al., Ferroptosis: an iron-dependent form of nonapoptotic cell death, Cell 149 (5) (2012) 1060–1072.
[20] A.D. Ladd, S. Duarte, I. Sahin, A. Zarrinpar, Mechanisms of drug resistance in HCC, Hepatology 79 (4) (2024) 926–940.
[21] Z. Lu, H. Yang, Y. Shao, W. Sun, Y. Jiang, J. Li, IGF2BP3-NRF2 axis regulates ferroptosis in hepatocellular carcinoma, Biochem. Biophys. Res. Commun. 627 (2022) 103–110.
[22] X. Li, Y. Li, W. Zhang, F. Jiang, L. Lin, Y. Wang, et al., The IGF2BP3/Notch/Jag1 pathway: a key regulator of hepatic stellate cell ferroptosis in liver fibrosis, Clin. Transl. Med. 14 (8) (2024) e1793.
[23] H. Sun, Y. Meng, L. Yao, S. Du, Y. Li, Q. Zhou, et al., Ubiquitin-specific protease 22 controls melanoma metastasis and vulnerability to ferroptosis through targeting SIRT1/PTEN/PI3K signaling, MedComm 5 (8) (2024) e684.
[24] J. Pan, W. Xiong, A. Zhang, H. Zhang, H. Lin, L. Gao, et al., The imbalance of p53-Park7 signaling axis induces iron homeostasis dysfunction in doxorubicin-challenged cardiomyocytes, Adv. Sci. (Weinh.) 10 (15) (2023) e2206007.
[25] A. Osmanovic, A. Förster, M. Widjaja, B. Auber, A.M. Das, A. Christians, et al., A SUMO4 initiator codon variant in amyotrophic lateral sclerosis reduces SUMO4 expression and alters stress granule dynamics, J. Neurol. 269 (9) (2022) 4863–4871.
[26] M.M. Souza, C.M. Coutinho-Camillo, F.M. de Paula, F. de Paula, S.B. Bologna, S. V. Lourenço, Relevant proteins for the monitoring of engraftment phases after allogeneic hematopoietic stem cell transplantation, Clinics 77 (2022) 100134.
[27] Y. Wang, Y. Wang, Y. Fang, H. Jiang, L. Yu, H. Hu, et al., SND1 regulates organic anion transporter 2 protein expression and sensitivity of hepatocellular carcinoma cells to 5-Fluorouracil, Drug Metab. Dispos. 52 (9) (2024) 997–1008.
[28] K.Z. Zhang, J.W. Li, J.S. Xu, Z.K. Shen, Y.S. Lin, C. Zhao, et al., RBP4 promotes denervation-induced muscle atrophy through STRA6-dependent pathway, J. Cachexia Sarcopenia Muscle 15 (4) (2024) 1601–1615.
[29] S. Doll, F.P. Freitas, R. Shah, M. Aldrovandi, M.C. da Silva, I. Ingold, et al., FSP1 is a glutathione-independent ferroptosis suppressor, Nature 575 (7784) (2019) 693–698.
[30] K. Li, C. Lin, M. Li, K. Xu, Y. He, Y. Mao, et al., Multienzyme-like reactivity cooperatively impairs glutathione peroxidase 4 and ferroptosis suppressor protein 1 pathways in triple-negative breast cancer for sensitized ferroptosis therapy, ACS Nano 16 (2) (2022) 2381–2398.
[31] C. Miao, Y. Huang, C. Zhang, X. Wang, B. Wang, X. Zhou, et al., Post-translational modifications in drug resistance, Drug Resist. Updates 78 (2025) 101173.
[32] S.C. Osmanoğulları, M. Forough, Ö. Persil Çetinkol, Y. Arslan Udum, L. Toppare, Electrochemical detection of oxaliplatin induced DNA damage in G-quadruplex structures, Anal. Biochem. 671 (2023) 115149.
[33] M. Hashemi, N. Esbati, M. Rashidi, S. Gholami, R. Raesi, S.S. Bidoki, et al., Biological landscape and nanostructural view in development and reversal of oxaliplatin resistance in colorectal cancer, Transl. Oncol. 40 (2024) 101846.
[34] H. Jin, L. Wang, R. Bernards, Rational combinations of targeted cancer therapies: background, advances and challenges, Nat. Rev. Drug Discov. 22 (3) (2023) 213–234.
[35] H. Chen, Y. Li, H. Li, X. Chen, H. Fu, D. Mao, et al., NBS1 lactylation is required for efficient DNA repair and chemotherapy resistance, Nature 631 (8021) (2024) 663–669.
[36] F. Tang, D. Xiao, X. Li, L. Qiao, The roles of lactate and the interplay with m(6)A modification in diseases, Cell Biol. Toxicol. 40 (1) (2024) 107.
[37] B.R. Stockwell, Ferroptosis turns 10: emerging mechanisms, physiological functions, and therapeutic applications, Cell 185 (14) (2022) 2401–2421.
[38] D. Wu, C.B. Spencer, L. Ortoga, H. Zhang, C. Miao, Histone lactylation-regulated METTL3 promotes ferroptosis via m6A-modification on ACSL4 in sepsis-associated lung injury, Redox Biol. 74 (2024) 103194.
[39] H. She, Y. Hu, G. Zhao, Y. Du, Y. Wu, W. Chen, et al., Dexmedetomidine ameliorates myocardial ischemia-reperfusion injury by inhibiting MDH2 lactylation via regulating metabolic reprogramming, Adv. Sci. (Weinh.) 11 (48) (2024) e2409499.
[40] J. Nerusch, G. Schicht, N. Herzog, J.H. Küpper, D. Seehofer, G. Damm, Investigation and distinction of energy metabolism in proliferating hepatocytes and hepatocellular carcinoma cells, Cells 14 (16) (2025) 1254.
[41] J. Gautam, J. Wu, J.S.V. Lally, J.D. McNicol, R. Fayyazi, E. Ahmadi, et al., ACLY inhibition promotes tumour immunity and suppresses liver cancer, Nature (2025).
[42] Y. He, T. Song, J. Ning, Z. Wang, Z. Yin, P. Jiang, et al., Lactylation in cancer: mechanisms in tumour biology and therapeutic potentials, Clin. Transl. Med. 14 (11) (2024) e70070.
[43] J. Jiang, D. Huang, Y. Jiang, J. Hou, M. Tian, J. Li, et al., Lactate modulates cellular metabolism through histone lactylation-mediated gene expression in non-small cell lung cancer, Front. Oncol. 11 (2021) 647559.
[44] Y. Wang, H. Li, S. Jiang, D. Fu, X. Lu, M. Lu, et al., The glycolytic enzyme PFKFB3 drives kidney fibrosis through promoting histone lactylation-mediated NF-κB family activation, Kidney Int. 106 (2) (2024) 226–240.
[45] Y. Li, Q. Cao, Y. Hu, B. He, T. Cao, Y. Tang, et al., Advances in the interaction of glycolytic reprogramming with lactylation, Biomed. Pharmacother. 177 (2024) 116982.
[46] R. Du, Y. Gao, C. Yan, X. Ren, S. Qi, G. Liu, et al., Sirtuin 1/sirtuin 3 are robust lysine delactylases and sirtuin 1-mediated delactylation regulates glycolysis, iScience 27 (10) (2024) 110911.
[47] H. Shen, X. Qi, Y. Hu, Y. Wang, J. Zhang, Z. Liu, et al., Targeting sirtuins for cancer therapy: epigenetics modifications and beyond, Theranostics 14 (17) (2024) 6726–6767.
[48] F. Lind-Holm Mogensen, A. Scafidi, A. Poli, A. Michelucci, PARK7/DJ-1 in microglia: implications in parkinson's disease and relevance as a therapeutic target, J. Neuroinflammation 20 (1) (2023) 95.
[49] T. Guo, L. Zhou, M. Xiong, J. Xiong, J. Huang, Y. Li, et al., N-homocysteinylation of DJ-1 promotes neurodegeneration in parkinson's disease, Aging Cell 23 (5) (2024) e14124.
[50] W. Jin, Novel insights into PARK7 (DJ-1), a potential anti-cancer therapeutic target, and implications for cancer progression, J. Clin. Med. 9 (5) (2020).
[51] H. Wang, H. Liu, X. Tang, G. Lu, S. Luo, M. Du, et al., Potentially functional variants of PARK7 and DDR2 in ferroptosis-related genes predict survival of non-small cell lung cancer patients, Int. J. Cancer 156 (4) (2025) 744–755.
[52] K. Pfister, V. Young, B. Frankel, A. Silva Barbosa, J. Burton, J. Bons, et al., Succinylation of Park7 activates a protective metabolic response to acute kidney injury, Am. J. Physiol. Ren. Physiol. 327 (1) (2024) F128–f136.